small
NANO MICRO

Nanopores

Automated Fabrication of 2-nm Solid-State Nanopores for Nucleic Acid Analysis

*Kyle Briggs, Harold Kwok, and Vincent Tabard-Cossa**

We demonstrate the automated and reproducible fabrication of sub-2-nm nanopores in 10-nm thick silicon nitride membranes, through controlled dielectric breakdown in solution. Our results reveal that under the appropriate conditions, nanopores can be fabricated with a size no larger than 2.0 ± 0.5-nm in diameter for a sample of N = 23 nanopores, with an average and standard deviation of 1.3 ± 0.6-nm. The dimensions of these nanopores are confirmed by using individual translocating DNA molecules as molecular rulers. We show that a 2.0-nm and a 2.1-nm diameter nanopore are capable of distinguishing single-stranded DNA versus double-stranded DNA, and that a 2.4-nm diameter nanopore can be used to investigate the overstretching transition in short dsDNA fragments. These results highlight the reliability and precision of the automated fabrication of nanopores via controlled dielectric breakdown, showing great promise for the manufacturing of future nanopore-based technologies.

1. Introduction

The utility of nanopores as single-molecule sensors is well-established, and relies on electrophoretically driving a charged analyte through the nanopore in an electrolyte solution while monitoring changes in the ionic current.[1–4] For nucleic acid analysis, it is often essential for the DNA molecule to pass through the pore in a single-file, sequential, manner. For this reason, nanopores with diameter comparable to that of DNA are crucial. At the same time, the sensitivity of the sensor also improves as its size approaches that of the analyte of interest.

The atomically precise structure of biological pores, such as α-Hemolysin and MspA, has, in part, contributed to their success in sequencing DNA strands, and at least in the short-term makes them more attractive for the commercialization of nanopore-based technologies.[5–7] Yet, compared to their organic counterparts, solid-state nanopore devices possess many attributes advantageous for the development of clinical diagnostic tools for personalized medicine applications and have been developed as an alternative.[8] Solid-state nanopores offer: a tunable pore size; increased stability over a wide range of operating conditions (pH, voltage, temperature); mechanical robustness; and a natural propensity for integration with semiconductor and microfluidics technologies. However, reliable fabrication of nanopores in thin solid-state membranes which are small enough to ensure single-file passage of double stranded DNA (dsDNA) and single-stranded DNA (ssDNA) has been challenging. While techniques for fabricating nanopores in the sub-5-nm range exist, either based on transmission electron microscope (TEM)[9,10] or ion-beam sculpting machine,[11] they are time-consuming, labor intensive, and have low yield. Typically, beams of high-energy particles cannot be focused tightly enough to reliably achieve 2-nm nanopores. Larger pores must therefore be shrunk through localized melting of the membrane in order to achieve the desired pore size,[9] though at the cost of locally modifying the membrane material composition.[12,13] In addition, for the case of the widely used TEM-based drilling, the nanopore creation is detected by eye, monitoring flickering on a fluorescent screen, confounding automation.

K. Briggs, H. Kwok, Prof. V. Tabard-Cossa
University of Ottawa
Ottawa, Ontario, Canada
E-mail: tcossa@uOttawa.ca

DOI: 10.1002/smll.201303602

In spite of these difficulties, small nanopores with dimensions ranging from 1.5-nm to 5-nm are being fabricated and used by a few research groups. Sub 2-nm nanopores are capable of directly affecting DNA structure and probing unzipping mechanics.[14] Another interesting observation was that the kinetics of DNA translocation was found to be qualitatively different as the nanopore size decreases, revealing much longer dwell times, highlighting the importance of DNA-pore interactions (i.e. friction) in the translocation dynamics.[15,16] The ability of small nanopores to detect DNA substructure also makes possible numerous medical diagnostic applications, including analytic drug screening through spatially resolved detection of DNA-biomolecule bound complexes.[17] More recently, it has been shown that small nanopores are capable of distinguishing short homopolymers from one another[18] and detecting DNA substructure,[19] moving one step closer to the goal of solid-state nanopore-based technologies for health related applications. Another study has demonstrated the utility of hafnium oxide as a robust membrane material for sub 2-nm nanopores which can be used to slow DNA translocations through interactions with the substrate.[20] Despite these impressive demonstrations, the pace of scientific discoveries employing small solid-state nanopores remains very limited by the low yield and complexity of the fabrication methods, which require extensive manual control from a highly trained user and numerous handling steps to prepare the nanopores, any part of which can damage the membrane. Consequently, commercially available 50-μm × 50-μm wide, 10-nm thick membranes are rarely used as they are far more likely to break, thus limiting fabrication to thicker membranes at the expense of a lower signal-to-noise ratio. Some groups overcome this difficulty by locally thinning part of a membrane,[21] though this adds multiple steps to the fabrication process, unavoidably affecting yield and increasing the time invested in fabrication.

Here, we show that fabrication by controlled dielectric breakdown can be used to reliably produce, in a simple and automated fashion, individual 2-nm nanopores in a 10-nm thick silicon nitride (SiN_x) membrane. We demonstrate a yield >95% by optimizing the fabrication conditions for the controlled breakdown of a dielectric membrane in an electrolyte solution.[22] The method relies on application of a sustained electric field across an insulating membrane in solution near its dielectric breakdown strength, which induces a localized leakage current through the membrane. By monitoring the resulting sustained tunneling current, the creation of a single nanopore is detected as an abrupt increase in the leakage current, which we attribute to the onset of ionic current. Small nanopores in thin membranes are obtained through feedback control at low to moderate voltages (~5–10V) to limit the damage to the membrane after the dielectric breakdown event. The current-voltage (I-V) characteristics of these nanopores over a ±1V range are measured in high salt concentration in order to minimize surface effects, which can cause current rectification, particularly for pores with diameters on the scale of the Debye length.[23,24] We employ the commonly used method of inferring nanopore size from conductance measurements, following Kowalczyk et al.[25]

$$G = \sigma\left(\frac{4L}{\pi d^2} + \frac{1}{d}\right)^{-1} \quad (1)$$

where σ is the solution conductivity, L the membrane thickness, d the pore diameter, and G the nanopore conductance, the validity of which has previously been demonstrated for nanopores fabricated by dielectric breakdown.[22] We demonstrate that nanopores produced in this way are excellent single-molecule detectors, capable of distinguishing ssDNA from dsDNA or probing tertiary structure in dsDNA. These results also serve to validate the accuracy of the nanopore size extracted from the conductance-based model.

2. Results and Discussion

2.1. Fabrication of sub 2-nm Nanopores

While our previous work with nanopores established the possibility of creating a single sub 2-nm nanopore in a thin silicon nitride membrane, parameters were not optimized for their reproducible automated fabrication. To demonstrate that nanofabrication by dielectric breakdown can consistently achieve nanopores smaller than 2-nm in diameter, we performed a systematic study under a specific set of fabrication conditions.

Prior to pore fabrication, 10-nm thick SiN_x membranes are cleaned in oxygen plasma for 30s at 30W to ensure a uniformly clean surface and to facilitate wetting of the membrane. We fabricate nanopores in 1M KCl or NaCl solution buffered at pH 10 with a trans-membrane potential difference of -8V. Once the leakage current, $I_{leakage}$, exceeds a threshold, I_{cutoff}, defined as $\frac{I_{cutoff}}{I_{leakage}} = 1.2 \pm 0.1$, the applied voltage is terminated at a response rate of 10Hz. These conditions are generally sufficient to limit the time between pore creation and voltage termination to <0.5 s. The typical time-to-pore creation in these conditions is ~10 minutes.

Immediately after creation, nanopores fabricated in this way typically exhibit some degree of rectification, self-gating, or significant levels of low-frequency (1/*f*-type) noise. As described in work by Beamish *et al*,[26] a moderate electric field strength in the range of ±0.2–0.3 V/m can be used rapidly mitigate these issues. However, we have found that this approach generally results in significant enlargement of the pore diameter. For this study, to ensure the fabrication of nanopores of the smallest diameter with low 1/*f*-type noise and ohmic behavior, we simply switched the solution to 3.6M LiCl buffered at pH 8 and allowed the nanopore to equilibrate for a few hours after fabrication. We have found this to be an effective way to improve the electrical characteristics of our nanopores. All I-V curves improve steadily in these conditions, showing an ohmic response within a few hours. **Figure 1** presents the time-evolution of the I-V characteristics of a nanopore as a function of immersion time in 3.6M LiCl pH 8, showing progressive improvement from a rectifying and self-gating pore to a well-behaved, ohmic nanopore. Nanopores left in 3.6M LiCl pH 8 overnight usually grow <1-nm. Note that nanopores drilled with a TEM

small 2014,
DOI: 10.1002/smll.201303602

NANO MICRO small

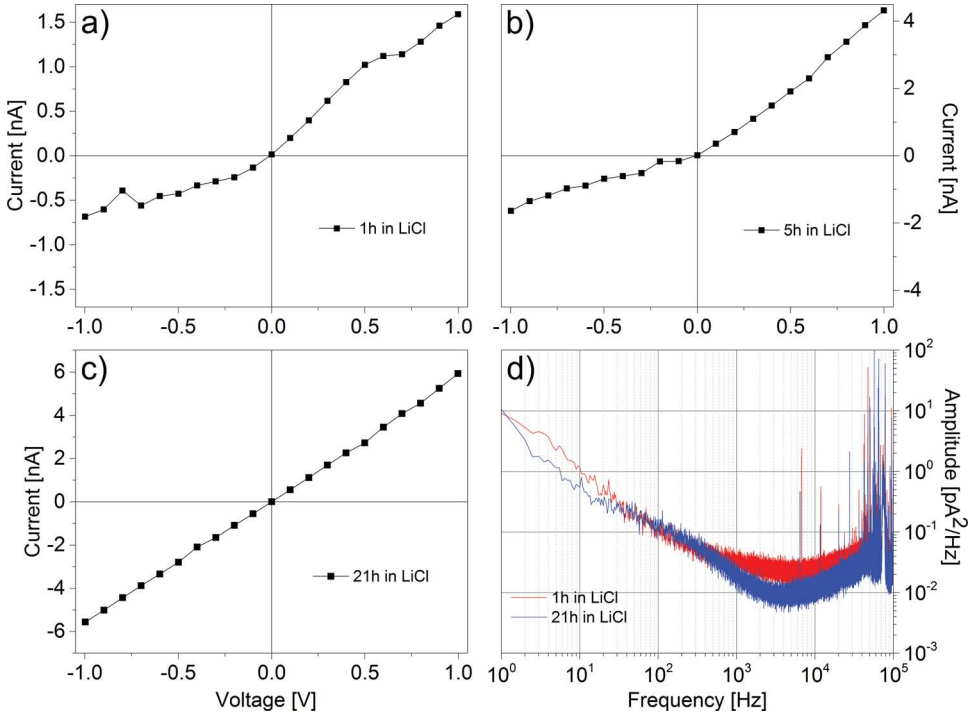

Figure 1. Time evolution of I-V characteristics for a nanopore immersed in 3.6M LiCl pH8. No other action was performed except for the periodic *I–V* curve measurements ramped from −1V and +1V. a) After 1 hour, G_+ = 1.54-nS, G_- = 0.59-nS, rectification ratio of 2.6; b) after 5 hours, G_+ = 4.4-nS, G_- = 1.57-nS, rectification ratio of 2.8; c) after 21 hours, G_{pore} = 5.68-nS, pore is ohmic. Estimated final size from conductance model is 2.3-nm. Note that vertical scales differ on all three graphs. d) Power spectrum density for the ionic current signal captured at +200mV, showing marginal improvement to noise despite increased current passage over the duration of nanopore equilibration.

also generally show conductance increasing over time, at a rate which can be significantly higher than observed here.[12] **Figure 2**a shows I-V curves of 5 independent nanopores fabricated via controlled dielectric breakdown once their I-V characteristics showed an ohmic response, within the first 24 hours after creation. We have found that all pores fabricated for this study showed similar electrical behaviors. These nanopores are also relatively stable over time, showing on average a growth rate of 0.4nm/day (N = 4, for a period of 4 days) at room temperature in 3.6M LiCl pH 8, with most of the growth concentrated in the first day. Remarkably, our results show that under the conditions described above we can fabricate nanopores no larger than 2.0 ± 0.5-nm in diameter for a sample of N = 23 nanopores (N = 19 in KCl, N = 4 in NaCl), with an average and standard deviation of 1.3 ± 0.6 nm. The distribution of initial nanopore sizes is shown in Figure 2b.

To achieve these results, we have identified two key conditions to reproducibly create small nanopores. First, the applied voltage must be rapidly reduced or turned off upon detection of the first discrete breakdown event, to avoid significant nanopore growth.[26] Secondly, the use of thinner membranes (e.g. 10-nm thick SiN_x) should be favored to minimize the variability in the damage size as a result of the dielectric breakdown event. Indeed, we have observed that although the fabrication of sub-2-nm nanopores is possible on 30-nm thick SiN_x membranes, the width of the distribution of fabricated size is larger. Once these conditions have been met, the choice of electrolyte solution used for fabrication plays a secondary role in the overall nanopore characteristics. We have found that using 1M KCl pH 10 as the fabrication solution gives reliable results, showing a clearer indication of a nanopore creation event and less initial ionic current rectification than other experimental conditions.

Under these fabrication conditions, pore enlargement after the discrete breakdown event is slow enough that a tighter cutoff or faster response time is not necessary to achieve 2-nm diameter nanopores. In principle, more rapid (10^{-3} vs. 10^{-1} seconds) response time and finer control could be achieved if it were necessary. The slightly extended tail toward larger pore sizes in Figure 2b is a direct consequence of the loose cutoff conditions used ($\frac{I_{cutoff}}{I_{leakage}} = 1.2 \pm 0.1$ and 0.1s response time), and the distribution could be made even narrower if an application demanded it.

2.2. dsDNA and ssDNA as Molecular Rulers

In order to establish the accuracy of the effective nanopore size extracted from the conductance-based model (Equation (1), we demonstrate the translocation of 50-nt fragments of single-stranded DNA (ssDNA) and 50-bp fragments of double-stranded DNA (dsDNA) through nanopores, which were measured at only slightly larger than the nominal diameter of the type of DNA in solution. In particular, we demonstrate successful translocation of ssDNA ($d_{ss} \approx$ 1.4-nm) through nanopores measured at 2.0-nm ± 0.2-nm and 2.1-nm ± 0.2-nm, which can barely pass dsDNA ($d_{ds} \approx$ 2.2-nm), and successful dsDNA translocation through a nanopore measured at 2.4-nm ± 0.2-nm. All translocation experiments are

DOI: 10.1002/smll.201303602

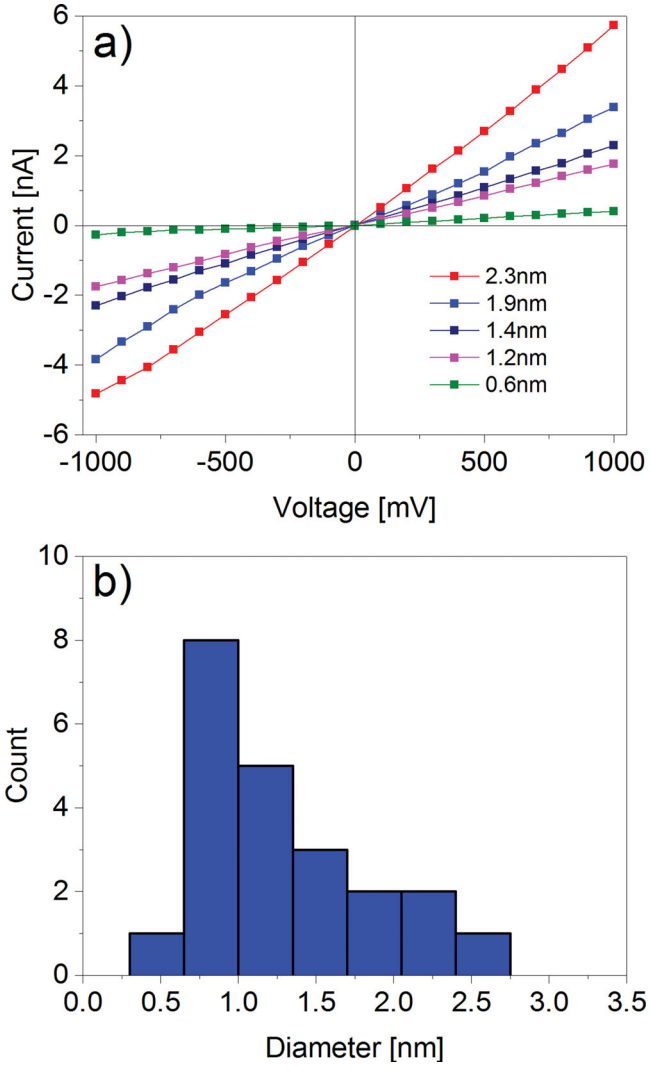

Figure 2. a) I-V curves of fabricated nanopores ranging in size from 0.6-nm to 2.3-nm, after aging for up to 24h in 3.6M LiCl pH 8. Based on Equation (1), a 1.5-nm nanopore has a conductance of 2.54-nS, a 2-nm nanopore has a conductance of 4.4-nS, while a 2.5-nm pore has a conductance of 6.60-nS. b) 0.35-nm bin histogram of the initial size of the fabricated nanopores, measured after allowing 1 hour of equilibration in 3.6 M LiCl pH 8, as determined from a conductance-based model,[25] which assumes a cylindrical geometry. In the case of rectification, size is inferred from the polarity of highest conductance.

carried out in 3.6 M LiCl pH 8 in order to maximize passage times[27] and to suppress surface effects.

We first investigate the translocation kinetics of DNA through a 2.0-nm nanopore as inferred from Equation (1). In order to avoid contamination or ambiguity between which species is being translocated, dsDNA and ssDNA are added to opposite sides of the membrane, and the fluid reservoirs are biased appropriately to drive negatively charged DNA though the nanopore. Since the diameter of this particular nanopore should be too small to allow dsDNA to pass, the attempt is first made to translocate dsDNA at –100 mV and –200 mV. **Figures 3**a and 3b show current traces before and after addition of both types of DNA on opposite sides of the membrane at a concentration of 50 nM. The baseline current is stable before addition of any DNA, showing no transient fluctuations during a control lasting 180 seconds. Upon addition of 50-bp dsDNA, very long (~seconds) single-molecule events are observed, which fully block the nanopore (>95% blockage). In the reverse voltage polarity, 50-nt ssDNA is observed to translocate readily, with an average of ~70% blockade level, as shown in Figure 3c and 3d. The scatter plot of the conductance blockages as a function of the translocation times, shown in Figure 3d, shows a slightly higher blockade than expected from a bulk excluded area argument in a solution of conductivity σ through a membrane of length L given by:[28,29]

$$\Delta G = \frac{\sigma \pi d_{DNA}^2}{4L} \quad (2)$$

which predicts a blockage of 2.5-nS, whereas the average blockage level observed is 3.1-nS for 245 single-molecule translocation events. We discuss this small discrepancy below.

In the dsDNA experiment shown in Figure 3, while it is clear from the presence of fully blocked events that dsDNA molecules are indeed interacting with the nanopore, the events are so long (seconds to minutes, in some cases) that it is unlikely that they represent full translocations. Moreover, if dsDNA translocated on that timescale, one might expect that reversing the voltage polarity during an event would result in a roughly comparable length of time before the nanopore returned to its open conductance state. This is not observed, and reversing the polarity immediately unblocks the pore, suggesting that dsDNA intercalates at the entrance of the pore, but is most probably not fully threaded at the voltages attempted (–100 mV and –200 mV). On the other hand, ssDNA translocates readily once the voltage reaches +200 mV. The dwell times in Figure 3d are nevertheless surprisingly long given the short length of the ssDNA strands (~25-nm), and corresponds to an exponential distribution with a characteristic time of 170-μs. Note that the notion of conserved equivalent charge deficit (e.c.d) no longer applies, and instead the general trend is for increasing dwell time with increasing conductance blockade. This behavior has been observed by several other groups working with solid-state nanopores of similar diameter, and is generally attributed to friction and other short-range pore-analyte interactions.[15,16] A control experiment (data not shown), translocating ssDNA through a nanopore fabricated in the same conditions but enlarged to 4.5-nm in diameter, showed passage times which were much faster, nearing the resolution of our instrument, limited in bandwidth with a maximum low-pass filter of 100kHz, thus confirming that the reduced translocation times in small nanopores is a size effect, as in previous studies.[16,20,30]

Analysis of ssDNA translocation data at +200 mV, presented in Figure 3d, reveals no current levels associated with molecules threading in folded configurations, despite the fact that the persistence length of ssDNA in high molarity electrolyte is less than 1-nm.[31] The absence of folded events is another strong indication that this particular nanopore, estimated at 2.0-nm by the conductance model, has a highly circular opening, with a major axis of ranging between 1.5-nm and 2.2-nm, thus indicating a measurement error in the conductance model used to extract an effective size of

small 2014,
DOI: 10.1002/smll.201303602

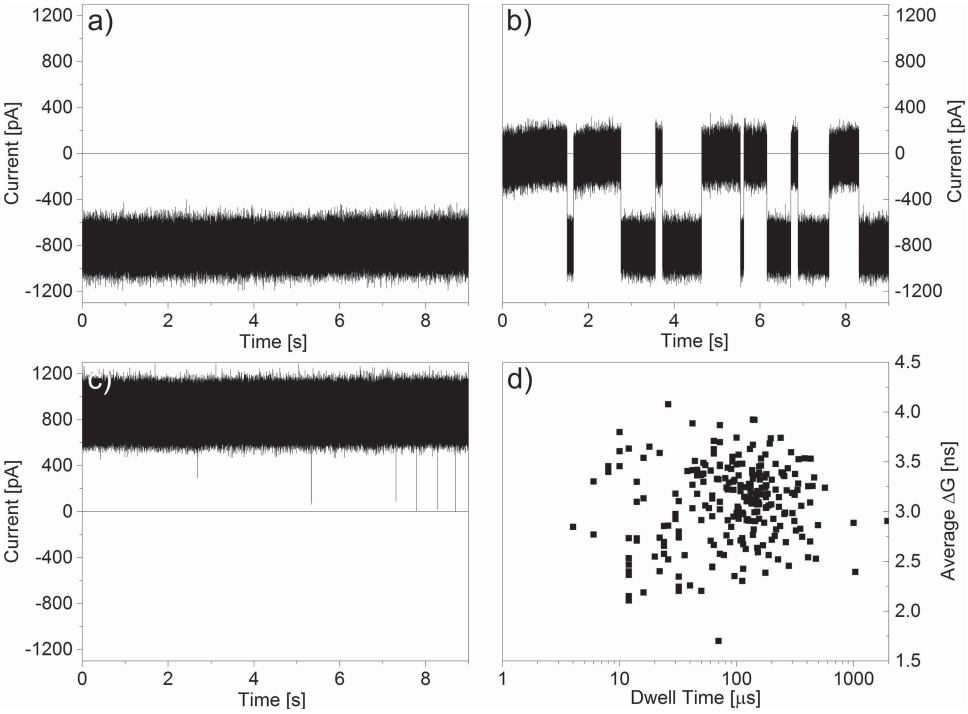

Figure 3. Current traces of a 2.0-nm diameter nanopore in 3.6M LiCl pH8 (nanopore conductance, G_{pore} = 4.5-nS) with a) no DNA at –200 mV, showing a clean baseline; b) 50nM 50-bp dsDNA at -200mV showing very long lasting events, which fully blocks the pore (residual current is ‹30 pA, within the noise), and c) 50nM 50-nt ssDNA at +200mV showing fast DNA translocation events with deep nanopore conductance blockades (~70% blockage); d) Scatter plot of conductance blockades versus dwell times for ssDNA translocation events (N = 245 events). Data was sampled at 500kHz and low-pass filtered at 100kHz.

± 0.5-nm. This is further supported by the fact that dsDNA can fully block the nanopore, which would not be possible if the minor axis of the nanopore diameter was less than 2.0-nm. The conductance blockade observed is on average slightly larger than the 2.5-nS predicted by the bulk model. We attribute this small discrepancy to uncertainties in the actual membrane thickness (nominally 10 ± 1-nm) and in the conductivity of the electrolyte inside the nanopore at this length scale. In addition, since electro-osmotic flow opposes DNA motion at this pH,[32] any interaction of the DNA with the electric double layer, which is unavoidable given the size of the nanopore, would tend to block more current than the bulk prediction. In order to properly include the surface contribution to the ionic current requires an accurate estimate of the surface charge of the nanopore, which is as yet unknown for this fabrication process. However, accounting for the surface charge contribution to Equation (1) would only reduce the extracted pore size, and the error incurred by ignoring it remains smaller than 0.5-nm[33] for these particular conditions over the typical range of surface charge values for silicon nitride.[34]

Next, we performed another set of experiments, under identical condition, on a different nanopore estimated at 2.1-nm in diameter by Equation (1). **Figure 4** displays ionic current traces showing individual 50-nt ssDNA translocation events for voltages between –200 mV and –800 mV. We observed thousands of single-molecule translocation events at each voltage. Note that, contrary to the previous study, no dsDNA translocations were observed at +200 mV. At +600mV, some transient, very small conductance blockages were observed, showing ca. 10% blockage, suggesting dsDNA collisions with the nanopore, but no threading.

Figure 5 presents analysis of the data acquired at various voltages in the form of semi-log density plots of conductance blockade versus dwell times for ssDNA translocation events. Similarly to the data acquired on the 2.0-nm nanopore, the relationship between dwell time and conductance blockage is not what one would expect for electrophoretically dominated translocation (the e.c.d is not conserved), showing weaker voltage dependence on the translocation time than the $t \propto V^{-1}$ observed for larger nanopores created in solution[22] and strong friction effects, and significantly weaker than the exponential dependence of dsDNA dwell time on voltage observed in small nanopores.[16,20] We attribute this difference to increased interactions between ssDNA and the nanopore than would be observed for dsDNA, which would lead to increased dwell times with a weaker voltage dependence. At –200 mV, we only observe single-level events with a distribution of blockade amplitudes and dwell times equivalent to the data shown in Figure 3d. Recall that the predicted blockage is 2.5-nS, whereas the average blockage level observed for this pore is 3.5-nS for N = 877 single-molecule translocation events. This compares well with the previous 2.0-nm nanopore studied. However, at higher voltages, another type of event is present, exhibiting a second deeper blockage level. These events, for which the ionic current trace resembles folded events, take much longer to translocate than their single-level counterparts. This is consistent with the notion of friction-dominated translocations, since folded events in such a small pore would force ssDNA to be

DOI: 10.1002/smll.201303602

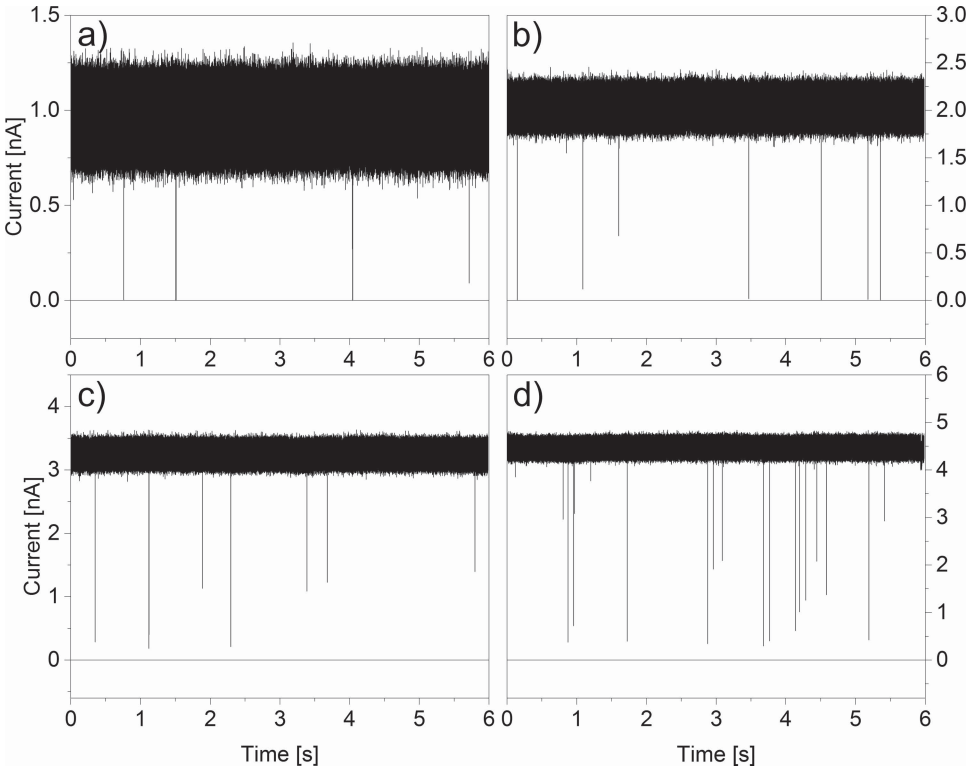

Figure 4. Current traces of ssDNA translocating a 2.1-nm nanopore (nanopore conductance 4.88-nS) in 3.6M LiCl pH8 at a) −200 mV, showing only single-level blockages with ~73% blockage b) −400 mV, showing two-level events with ~80% blockage and single-level events with ~60% blockage c) −600 mV, showing two-level events with ~80% blockage and single-level events with ~50% blockage and d) −800 mV, showing mainly single-level events with ~45% blockage. Current traces are multiplied by -1 for clarity. Data was acquired at 500kHz and low-pass filtered at 100kHz.

squeezed inside the nanopore and cause much stronger interactions with the nanopore. These folded events could indicate the possibility of a slightly more elliptically shaped opening for this particular pore, which could be as much as much as 1.4-nm × 2.8-nm while presenting the same cross-sectional area, and still preventing dsDNA passage. However, data at –200 mV suggests that the cylindrical model is valid and some previous TEM images of nanopores created via dielectric breakdown showed circular cross-sections.[22] Therefore, it may be more likely that we are simply able to force ssDNA though an opening smaller than its nominal diameter in solution by applying such high voltage. From Figure 5, it is clear that despite having a sub-linear voltage dependence, the dwell time of both the low and high conductance blockage states decreases with increasing voltage, consistent with full translocation events as opposed to intercalation. Also of note is the fact that the single level conductance blockage is voltage dependent, showing lower blockages with increasing voltage, consistent with previous studies showing ssDNA stretching with increasing voltages.[35]

Finally, we investigate the translocations of dsDNA (d_{ds} ≈ 2.2-nm) molecules through a nanopore measured at 2.4-nm in diameter to further ascertain the accuracy of the nanopore size extracted from the conductance-based model. At this size, dsDNA should barely thread through the nanopore, while maintaining its hybridized form. The experimental conditions are identical to those used for the ssDNA experiments described above. Ionic current traces exhibiting transient current blockades from individual translocating dsDNA molecules are presented in **Figure 6**. At all voltages we observe two types of events. Most events display a single deep conductance blockade level (ca. 98% blocked), while some exhibit two conductance levels, having first the same deep conductance level followed by a lower and longer blockage level, as shown in Figure 6e.

At –200 mV, the observed conductance blockage of the single-level events is 5.6-nS ± 0.4-nS, which is roughly consistent with the expected value of ΔG = 6.1nS for single file translocations of dsDNA, according to Equation (2). As the voltage is increased to –800 mV in 200 mV increments, the conductance blockage of the single-level events is gradually reduced. This is clearly observed in **Figure 7**, which shows a density plot of the observed conductance blockages versus dwell times at various voltages. Again, we observe the departure of translocation events from the line of conserved e.c.d and a dramatic increase in the translocation time over nanopores with >5-nm diameter made in similar conditions.[22] As seen in Figure 7e, the dwell time of dsDNA molecules follows an exponential dependence on voltage, consistent with previous work.[16,20] Dwell times are roughly log-normally distributed at each voltage, shown in Figure 7f, though there is a slightly heavy tail toward longer translocation times, indicative of DNA-nanopore interactions.

Although events consisting of two discrete conductance levels are reminiscent of folded DNA translocations, these cannot be folded events. Considering that the initial level is the expected conductance blockage for dsDNA (d_{ds}≈2.2-nm) entering the pore in a single file manner, the

small 2014,
DOI: 10.1002/smll.201303602

NANO MICRO small

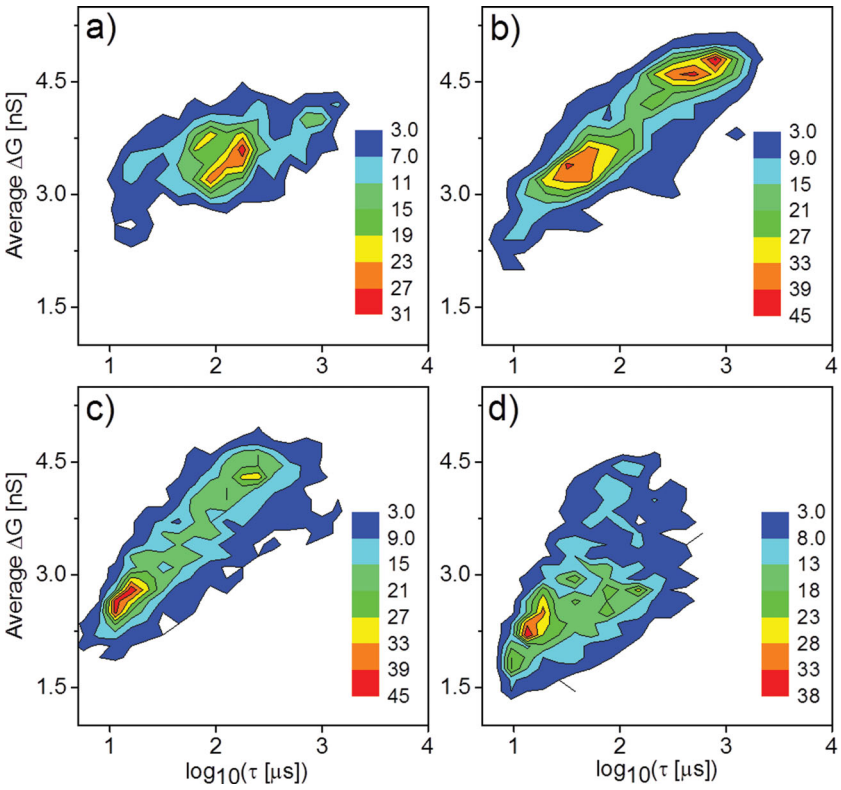

Figure 5. Semi-log event density plots of 50-nt ssDNA translocation events through a nanopore with an area equivalent to a 2.1-nm nanopore, with open pore conductance of 4.9-nS. a) Data acquired at −200 mV showing only one conductance blockade level (N = 877 events); b) Data acquired at −400 mV showing a second conductance blockade levels (N = 1290 events); c) Data acquired at −600 mV showing two conductance blockade levels (N = 1823 events); d) Data acquired at −800 mV showing two conductance blockade levels (N = 1685 events). Color scale indicates number of events. Data was digitized at 500kHz and low-pass filtered at 100kHz.

second blockage level, which is significantly smaller, must therefore be indicative of a narrower molecular state. Moreover, since the persistence length of 50-bp dsDNA is longer than the fragment size (50-nm vs. 18-nm), the molecule should essentially be rod-like, thus avoiding folded molecular conformations. Consequently, to explain our results, we propose that the nanopore is accessing the B-S stretching transition in dsDNA, in which a stretching force of ~65pN is sufficient to uncoil the double helix, resulting in a factor of 1.7 × increase in DNA strand length.[36–39] We argue that since the force is applied to both strands, the unzipping of the double helix is unlikely. First-order constant volume estimates suggest that an increase in DNA length should result in an equal decrease in cross-sectional area, and therefore conductance blockage, and predicts a conductance blockage of 3.6-nS for overstretched DNA. This is consistent with the most probable conductance level of these events, measured at 3.3-nS ± 0.4-nS at –600 mV (Figure 7c). We propose the following mechanism for the observed electrical signals: one end of the short dsDNA fragment is fully threaded inside the 2.4-nm nanopore but does not completely translocate, resulting in the deep blockade seen at the beginning of the two-level events. The dsDNA molecule is then temporarily trapped by the nanopore, resulting in the exceptionally long translocation time observed in all of the stretched DNA events. To first order, considering the nanopore is cylindrical, we expect a uniform electric field across its length. At 400 mV, we estimate the force experienced by a 10-nm segment of dsDNA, using

$$f(V) = ze\left(\frac{n}{L}\right)V \quad (3)$$

where $ze = -0.49e$ (inferred from Figure 4a in[40]) is the DNA effective charge in the nanopore per base pair, nL^{-1} is the inverse of the base-pair spacing of 0.34-nm for the B form of dsDNA. The calculated force is ~92pN, slightly above the range required to access the full extent of the B-S stretching transition, which is expected to occur above ~65pN.[36] However, note that not all the electrostatic pulling force is necessarily translated to a stretching force. For a translocating molecule the opposing force is provided by friction in the nanopore, which will always be less than the pulling force, unless the molecule is completely stalled. Moreover, there is a certain level of uncertainty with the value of the effective charge of DNA inside a nanopore,[41,42] which will affect the accuracy of the calculated pulling force, and as DNA is stretched, the linear charge density is reduced proportionately, reducing the stretching force. Thus, we would expect that the pulling force experienced by the DNA molecule must be somewhat higher than the required stretching force to access the stretching transition. The fact that the nanopore frequently shows deep and long lasting blockages which need to be cleared by reversing the voltage polarity attests to the strong likelihood that DNA can be temporarily trapped and stretched during translocation.

Of particular interest is the voltage dependence of the blockade events, which decreases with increasing applied voltage. The single-level conductance blockages approach the predicted 6.1nS at low voltage, as seen in Figure 7. We attribute this voltage-dependent behavior to stretching of the dsDNA segment inside the pore, but below the B-S overstretching transition. We argue that considering the increased translocation times, the significant DNA-pore interactions present will contribute to generate a substantial stretching force on the molecule, which can result in its elongation even if it does not reach the full stretching transition. The decreasing conductance blockage at higher voltages for the stretched events indicates stretching past the B-S plateau. We propose a similar explanation for the decreased conductance blockage with higher voltage observed for ssDNA as well (Figure 5). One would only expect to be able to see this behavior in pores small enough to cause appreciable friction

DOI: 10.1002/smll.201303602

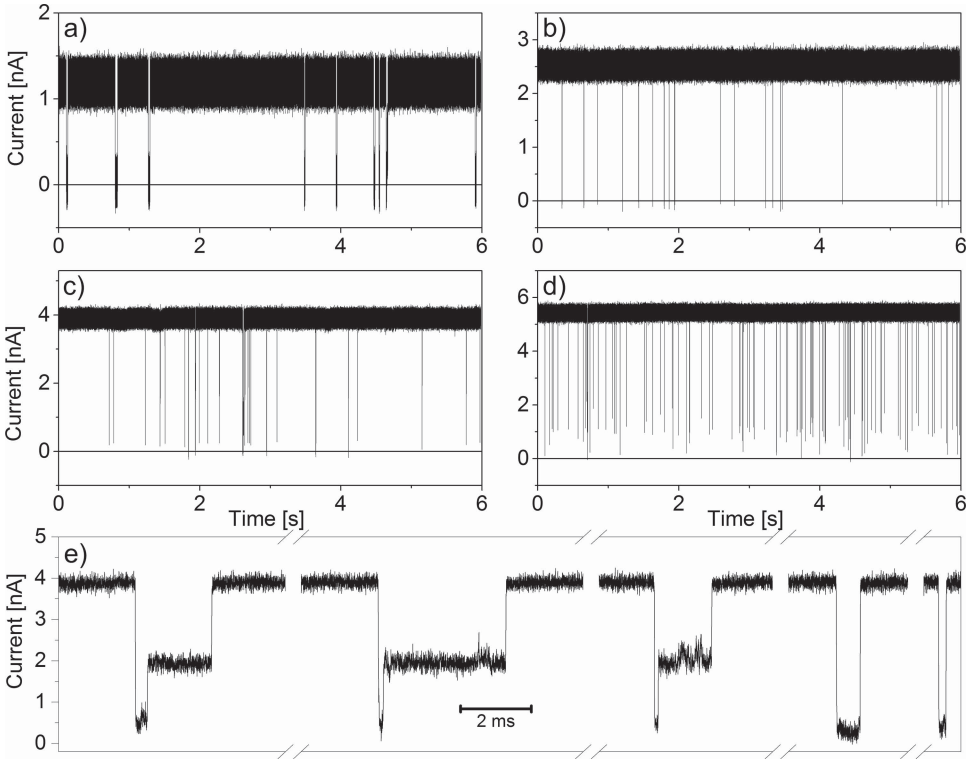

Figure 6. current traces for dsDNA translocating a 2.4-nm nanopore at a) −200 mV, showing mainly single-level events with complete pore blockage (residual current less than noise level) b) −400 mV, where stretched events begin to appear c) −600 mV, with the highest population of stretched events, and d) −800 mV, with a reduced stretched population. e) Examples of typical overstretched (two-level events) and unstretched (single-level events) dsDNA translocation events at −600 mV. Data was acquired at 500kHz and low-pass filtered at 100kHz. The recorded current is multiplied by -1 for clarity.

to provide the opposing force for stretching to occur. Such behavior has also been indirectly observed in nanopores slightly smaller than the diameter of dsDNA under higher voltage, consistent with this interpretation.[30]

In the absence of TEM images of every fabricated nanopore, the accuracy of the nanopore size inferred from the measured conductance can be questioned. The model relies on the assumption of no appreciable thinning of the membrane in the vicinity of the pore and a cylindrical geometry.[25] While in previous work we were able to confirm the first condition using simple excluded area arguments for DNA translocation, and the second condition through TEM images in the case of slightly larger nanopores,[22] it is not necessarily obvious that this conductance model of the nanopore would extend to such a small size regime while maintaining its accuracy. Remarkably, the results presented here strongly support these assumptions and the validity of the model. Using –200mV, we are able to pass dsDNA (d_{ds} = 2.2-nm) through nanopores, which we measured to be 2.4-nm ± 0.2-nm in diameter, but not through pores we measured to be 2.0-nm ± 0.2-nm and 2.1-nm ± 0.2-nm, showing that the accuracy of our extracted pore size can be in the angstrom range for the small nanopores fabricated for this work. However, we note one caveat. Due to the importance of electric double layer effects in sub-5-nm nanopores, the model is only accurate in the limit of high electrolyte concentration. For pores on the order of 2-nm, we have observed a systematic increase in measured nanopore size by as much as 30% when measured in 1M KCl as opposed to 3.6M LiCl. Given the close match between the measured pore diameters and the range of possible diameters predicted for passage of ss- and dsDNA, it is clear that the more accurate estimate comes from the higher salt concentration.[24,33]

3. Conclusion

We have demonstrated that systematic fabrication of solid-state nanopores in 10-nm thick silicon nitride membranes is possible using controlled dielectric breakdown in solution, achieving an average diameter of 1.3 ± 0.6-nm for a sample of N = 23 nanopores, through careful feedback control and automation of the fabrication process. Given that the fabrication conditions required are very general and non-specific to SiN_x, we expect this method to be readily applicable to other dielectric substrates, such as Al_2O_3 or HfO_2. The small nanopores created in this manner are excellent single-molecule sensors, showing clear, high signal-to-noise electrical signals and long, friction-dominated DNA translocation times. These translocation characteristics are consistent with that observed for nanopores of similar size fabricated with traditional TEM-drilling approach, though with a fraction of the effort and cost.

Given the intriguing dynamics accessible to sub 2-nm nanopores, we hope this work will spark further

small 2014,
DOI: 10.1002/smll.201303602

NANO MICRO small

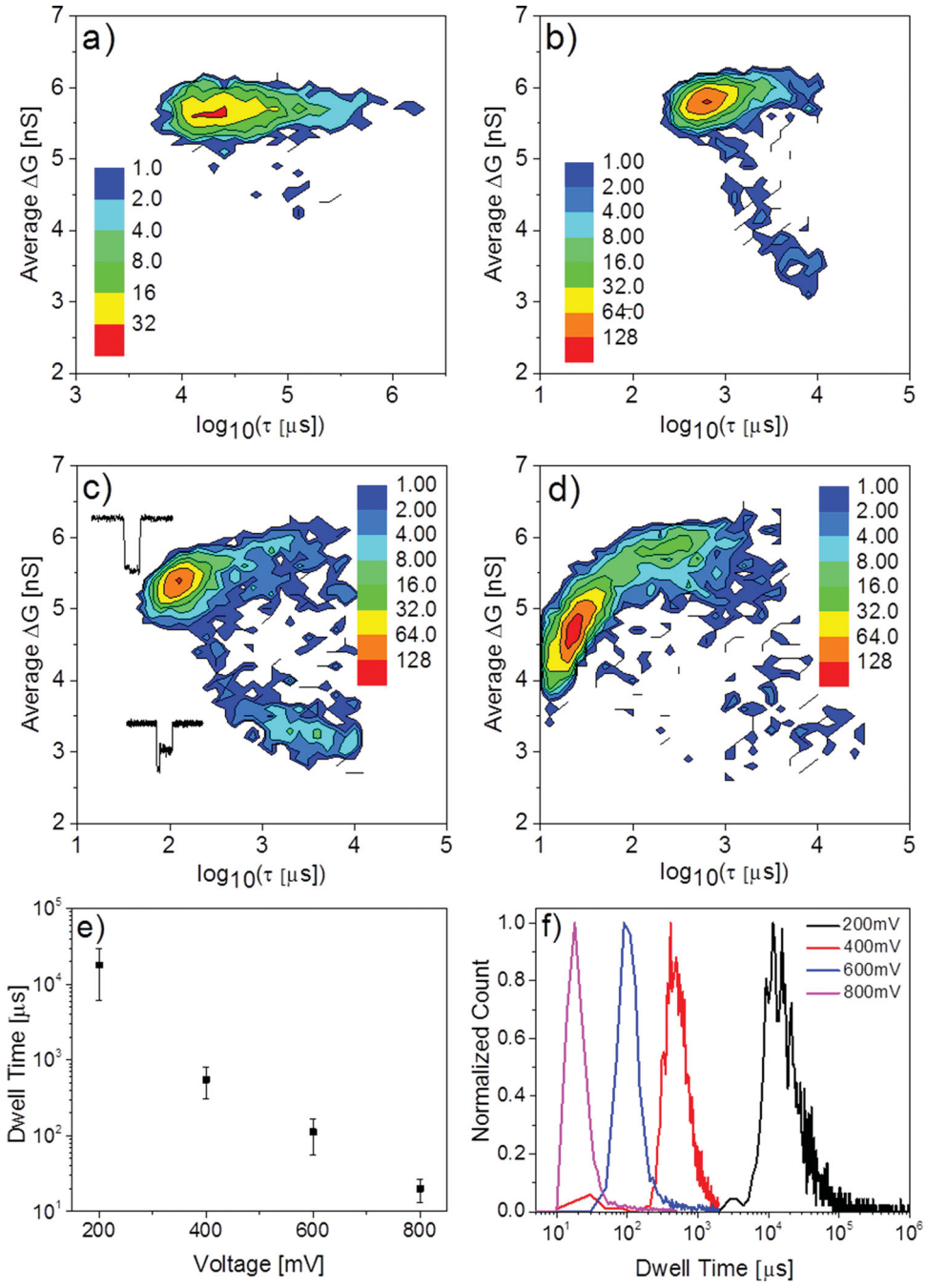

Figure 7. Scatter plot of 50-bp dsDNA translocation events through a 2.4-nm pore, with open pore conductance 6.3-nS. The expected conductance blockage for dsDNA is 6.1-nS, which is approached at low voltage. Reduced blockage levels with long dwell times are attributed to overstretched dsDNA. a) Data acquired at −200 mV (N = 1370 events, <1% show two-level events; b) Data acquired −400 mV (N = 2565 events, 5% show two-level events); c) Data acquired −600 mV (N = 2834 events, 14% show two-level events), inset shows typical events from each population; d) Data acquired -800mV (N = 5055 events, 2% show two-level events). Note the scale change between plots a) and b). Color scale indicates number of events. The dwell time dependence on voltage is shown in e), and the log-normal distribution of dwell time for each voltage is shown in f). Data was sampled at 500kHz and low-pass filtered at 100kHz.

investigations of the transport of nucleic acids and proteins through small solid-state nanopores by a wider range of researchers. We envision that the low-cost automated fabrication by dielectric breakdown of sub-2-nm nanopores with sub-nm precision will enable a more rapid development of solid-state nanopore-based technologies for personalized genomics.

4. Experimental Section

We fabricate nanopores in 10-nm low-stress SiN_x transmission electron microscope (TEM) windows purchased commercially from Norcada Inc. Membranes consist of SiN_x desposited on a Si substrate by low-pressure chemical vapor deposition (LPCVD). A 50 × 50-μm window is opened through the Si substrate with an

DOI: 10.1002/smll.201303602

anisotropic KOH etch to expose a free-standing area of SiN_x. To ensure the structural integrity of the membrane, voltage below 1V is applied to the membrane prior to nanopore creation to ensure no ionic current can pass. Fabrication is carried out following the method outlined in our previous work.[22] The salt used for fabrication is 1M KCl or NaCl pH 10 buffered with 10mM $NaHCO_3$, while the salt used in translocation experiments and for measuring nanopore size is 3.6M LiCl pH 8 buffered with 10mM HEPES. The etch pit side of the membrane is grounded and all voltages in this paper are referred from this ground.

Data is acquired using custom LabVIEW software interfacing with a National Instruments USB-6351 DAQ card. During nanopore fabrication, data is acquired at 250kHz and software-averaged to 10Hz. During DNA translocation experiments, data is acquired at 500kHz using an Axopatch 200B and hardware low-pass filtered at 100kHz using a 4-pole Bessel filter. All data analysis was done using custom LabVIEW software and Origin.

50bp dsDNA samples were purchased from Fermentas (NoLimits products, Thermo Scientific product #SM1421), and 50-nt ssDNA samples were purchased from Integrated DNA Technologies, Inc. The sequence of the ssDNA strands was $(A_9C)_5$.

Acknowledgments

This work was supported by the Natural Sciences and Engineering Research Council of Canada (NSERC), and the Canada Foundation for Innovation. K. Briggs acknowledges the financial support provided by NSERC (Postgraduate Fellowship). The authors would like to thank L. Andrzejewski for valuable technical support.

[1] D. Branton, D. W. Deamer, A. Marziali, H. Bayley, S. A. Benner, T. Butler, M. Di Ventra, S. Garaj, A. Hibbs, X. Huang, S. B. Jovanovich, P. S. Krstic, S. Lindsay, X. S. Ling, C. H. Mastrangelo, A. Meller, J. S. Oliver, Y. V Pershin, J. M. Ramsey, R. Riehn, G. V Soni, V. Tabard-Cossa, M. Wanunu, M. Wiggin, J. A. Schloss, *Nat. Biotechnol.* **2008**, *26*, 1146–53.
[2] B. M. Venkatesan, R. Bashir, *Nat. Nanotechnol.* **2011**, *6*, 615–24.
[3] J. J. Kasianowicz, J. W. F. Robertson, E. R. Chan, J. E. Reiner, V. M. Stanford, *Annu. Rev. Anal. Chem.* **2008**, *1*, 737–66.
[4] M. Wanunu, *Phys. Life Rev.* **2012**, *9*, 125–58.
[5] J. Clarke, H. Wu, L. Jayasinghe, A. Patel, S. Reid, H. Bayley, *Nat. Nanotechnol.* **2009**, *4*, 265–70.
[6] E. A. Manrao, I. M. Derrington, A. H. Laszlo, K. W. Langford, M. K. Hopper, N. Gillgren, M. Pavlenok, M. Niederweis, J. H. Gundlach, *Nat. Biotechnol.* **2012**, *30*, 349–53.
[7] I. M. Derrington, T. Z. Butler, M. D. Collins, E. Manrao, M. Pavlenok, M. Niederweis, J. H. Gundlach, *PNAS* **2010**, *107*, 16060–5.
[8] C. Dekker, *Nat. Nanotechnol.* **2007**, *2*, 209–15.
[9] A. J. Storm, J. H. Chen, X. S. Ling, H. W. Zandbergen, C. Dekker, *Nat. Mater.* **2003**, *2*, 537–40.
[10] A. J. Storm, J. H. Chen, X. S. Ling, H. W. Zandbergen, C. Dekker, *J. Appl. Phys.* **2005**, *98*, 014307.
[11] J. Li, D. Stein, C. McMullan, D. Branton, M. J. Aziz, J. A. Golovchenko, *Nature* **2001**, *412*, 166–9.
[12] M. van den Hout, A. R. Hall, M. Y. Wu, H. W. Zandbergen, C. Dekker, N. H. Dekker, *Nanotechnology* **2010**, *21*, 115304.
[13] A. S. Prabhu, K. J. Freedman, J. W. F. Robertson, Z. Nikolov, J. J. Kasianowicz, M. J. Kim, *Nanotechnology* **2011**, *22*, 425302.
[14] B. McNally, M. Wanunu, A. Meller, *Nano Lett.* **2008**, *8*, 3418–22.
[15] V. Kurz, E. M. Nelson, J. Shim, G. Timp, *ACS Nano* **2013**, *7*, 4057–69.
[16] M. Wanunu, J. Sutin, B. McNally, A. Chow, A. Meller, *Biophys. J.* **2008**, *95*, 4716–25.
[17] M. Wanunu, J. Sutin, A. Meller, *Nano Lett.* **2009**, *9*, 3498–502.
[18] K. Venta, G. Shemer, M. Puster, J. A. Rodríguez-Manzo, A. Balan, J. K. Rosenstein, K. Shepard, M. Drndić, *ACS Nano* **2013**, *7*, 4629–36.
[19] A. Singer, H. Kuhn, M. Frank-Kamenetskii, A. Meller, *J. Phys. Condens. Matter* **2010**, *22*, 454111.
[20] J. Larkin, R. Henley, D. C. Bell, T. Cohen-Karni, J. K. Rosenstein, M. Wanunu, *ACS Nano* **2013**, *7*, 10121–8.
[21] M. Wanunu, T. Dadosh, V. Ray, J. Jin, L. McReynolds, M. Drndić, *Nat. Nanotechnol.* **2010**, *5*, 807–14.
[22] H. Kwok, K. Briggs, V. Tabard-Cossa, *PLoS One* **2014**, *accepted*. *ArXiv 1310.5126*.
[23] E. C. Yusko, R. An, M. Mayer, *ACS Nano* **2010**, *4*, 477–487.
[24] Y. Liu, D. E. Huber, V. Tabard-Cossa, R. W. Dutton, *Appl. Phys. Lett.* **2010**, *97*, 143109.
[25] S. W. Kowalczyk, A. Y. Grosberg, Y. Rabin, C. Dekker, *Nanotechnology* **2011**, *22*, 315101.
[26] E. Beamish, H. Kwok, V. Tabard-Cossa, M. Godin, *Nanotechnology* **2012**, *23*, 405301.
[27] S. W. Kowalczyk, D. B. Wells, A. Aksimentiev, C. Dekker, *Nano Lett.* **2012**, *12*, 1038–44.
[28] D. Fologea, J. Uplinger, B. Thomas, D. S. McNabb, J. Li, *Nano Lett.* **2005**, *5*, 1734–1737.
[29] A. J. Storm, J. H. Chen, H. W. Zandbergen, C. Dekker, *Phys. Rev. E* **2005**, *71*, 051903.
[30] U. Mirsaidov, J. Comer, V. Dimitrov, A. Aksimentiev, G. Timp, *Nanotechnology* **2010**, *21*, 395501.
[31] H. Chen, S. P. Meisburger, S. A. Pabit, J. L. Sutton, W. W. Webb, L. Pollack, *Proc. Natl. Acad. Sci. USA* **2012**, *109*, 799–804.
[32] B. Luan, A. Aksimentiev, *J. Phys Condens. Matter* **2010**, *22*, 454123.
[33] R. M. M. Smeets, U. F. Keyser, D. Krapf, M.-Y. Wu, N. H. Dekker, C. Dekker, *Nano Lett.* **2006**, *6*, 89–95.
[34] M. Firnkes, D. Pedone, J. Knezevic, M. Do, U. Rant, *Nano Lett.* **2010**, *10*, 2162–2167.
[35] G. M. Skinner, M. van den Hout, O. Broekmans, C. Dekker, N. H. Dekker, *Nano Lett.* **2009**, *9*, 2953–60.
[36] S. B. Smith, Y. Cui, C. Bustamante, *Science* **1996**, *271*, 795–798.
[37] M. C. Williams, J. R. Wenner, I. Rouzina, V. a. Bloomfield, *Biophys. J.* **2001**, *80*, 874–81.
[38] X. Zhang, H. Chen, H. Fu, P. S. Doyle, J. Yan, *PNAS* **2012**, *109*, 8103–8.
[39] H. Fu, H. Chen, X. Zhang, Y. Qu, J. F. Marko, J. Yan, *Nucleic Acids Res.* **2011**, *39*, 3473–81.
[40] S. van Dorp, U. F. Keyser, N. H. Dekker, C. Dekker, S. G. Lemay, *Nat. Phys.* **2009**, *5*, 347–351.
[41] J. Zhang, B. Shklovskii, *Phys. Rev. E* **2007**, *75*, 021906.
[42] B. Luan, A. Aksimentiev, *Phys. Rev. E* **2008**, *78*, 021912.

Received: November 20, 2013
Revised: January 14, 2014
Published online:

DOI: 10.1002/smll.201303602